Facile synthesis of metal-free N-doped carbon electrocatalyst for selective CO_2-to-CO conversion from acetone aldol reaction products

Kou Adachi[1], Ryuji Takada[1,], Koji Miyake[1,2,*], Yoshiaki Uchida[1], Norikazu Nishiyama[1,2]*

[1] Division of Chemical Engineering, Graduate School of Engineering Science, Osaka University, 1-3 Machikaneyama, Toyonaka, Osaka 560-8531, Japan

[2] Innovative Catalysis Science Division, Institute for Open and Transdisciplinary Research Initiatives (ICS-OTRI), Osaka University, Suita 565-0871, Japan

* Corresponding Authors. E-mail: r.takada@cheng.es.osaka-u.ac.jp, kojimiyake@cheng.es.osaka-u.ac.jp

Table S1 The yields of catalysts

Catalyst	Mass of precursor (mg)	Mass of NH_4Cl (mg)	Mass of catalysts (mg)	Yield (%)
C-1000	300.00	-	25.51	5.44
CN-900	300.00	300.00	46.93	7.82
CN-1000(CN-1)	300.00	300.00	21.34	3.56
CN-1100	300.00	300.00	17.85	2.98
CN-1200	300.00	300.00	13.45	2.24
CN-0.5	300.00	150.00	18.71	4.16
CN-2	300.00	600.00	20.99	2.33
CN-3	300.00	900.00	19.27	1.60

calculated by the following equation:

$$Yield(\%) = \frac{Mass\ of\ catalyst}{Mass\ of\ precursor + Mass\ of\ NH_4Cl} \times 100$$

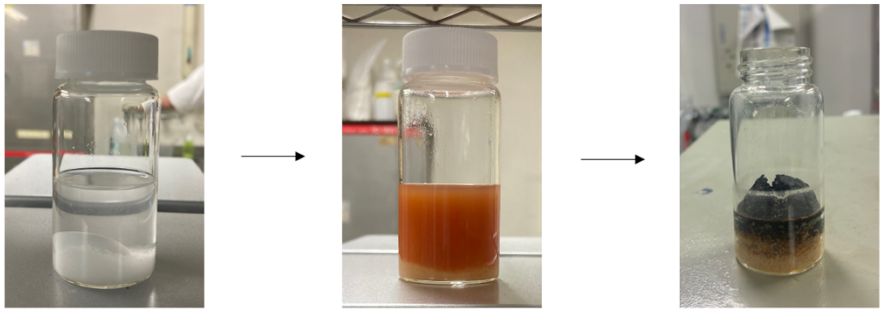

Fig. S1 Photographs showing the progression of the Aldol reaction and the formation of precursors.

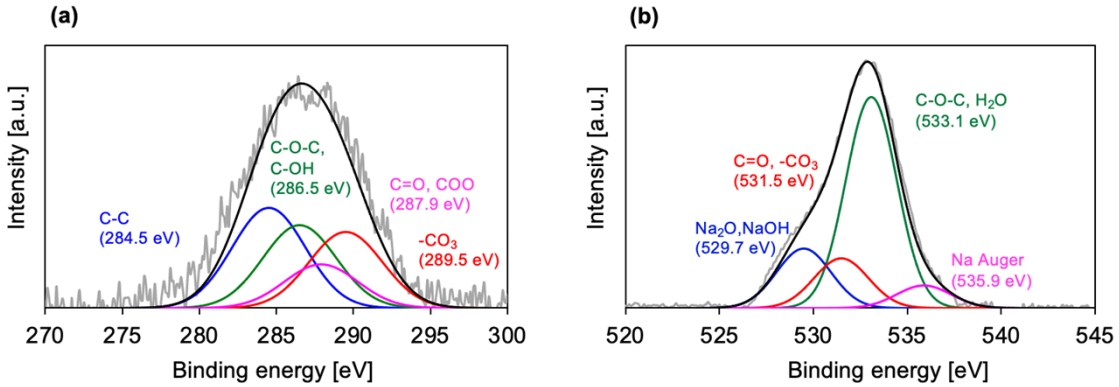

Fig. S2 C 1s[1,2] and O 1s XPS[1,3,4] spectra of precursors.

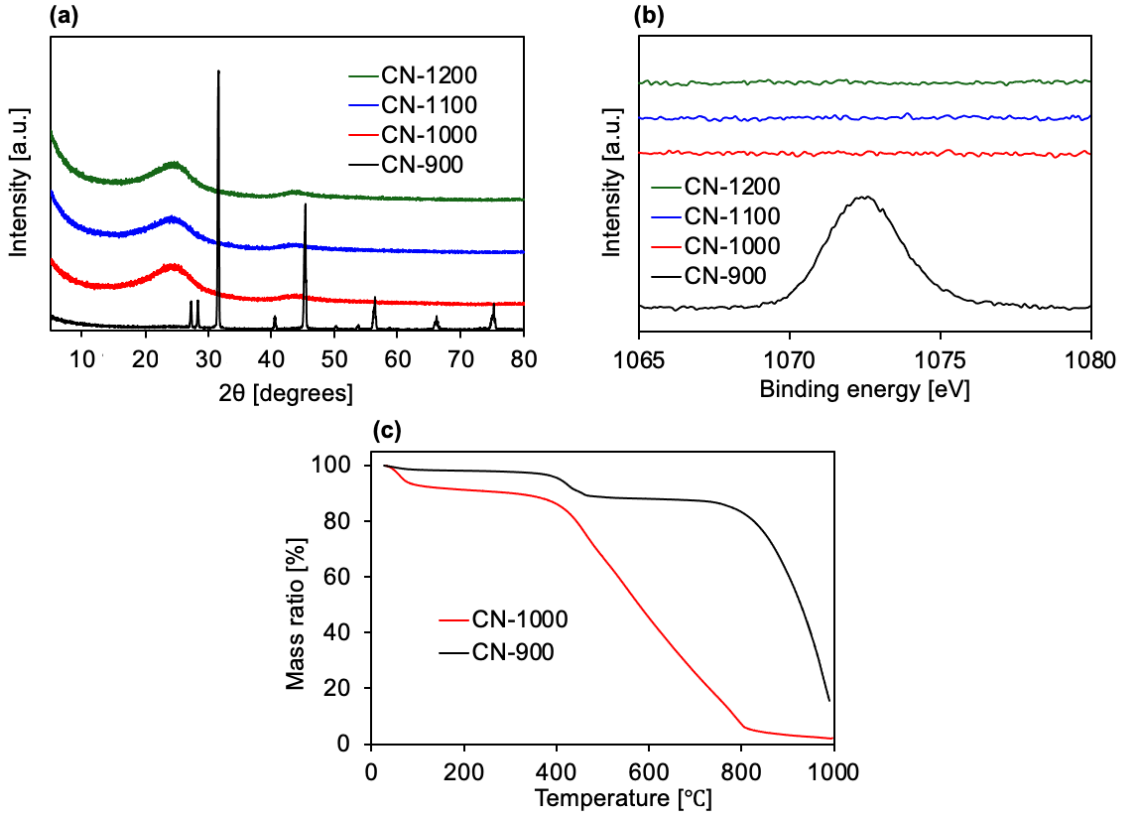

Fig. S3 (a) XRD patterns, (b) the Na 1s XPS spectra of CN-*T* and (c) TG curves of CN-900 and CN-1000, performed under air flow.

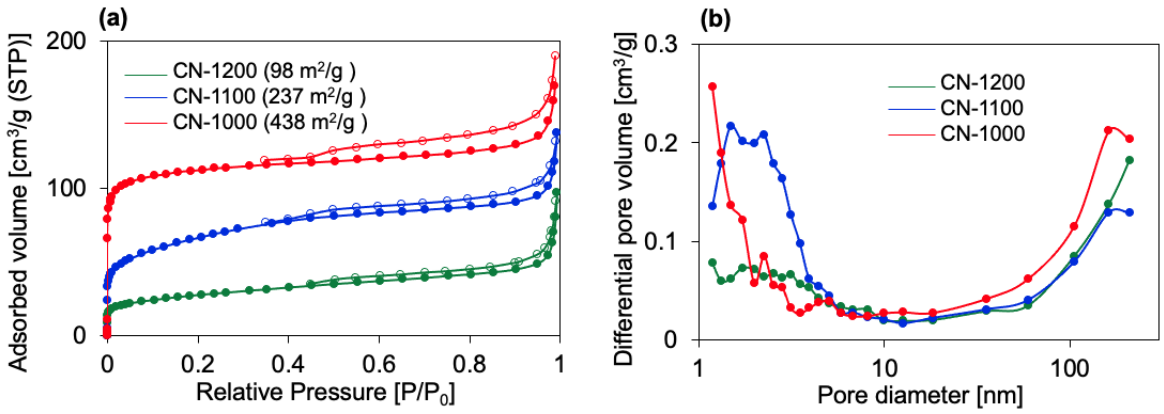

Fig. S4 (a) N_2 adsorption and desorption isotherms and (b) pore size distributions of CN-*T*

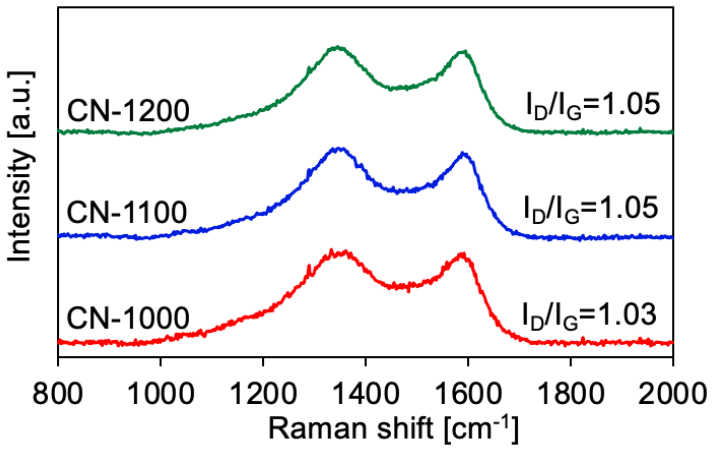

Fig. S5 Raman spectroscopy analysis of CN-*T*.

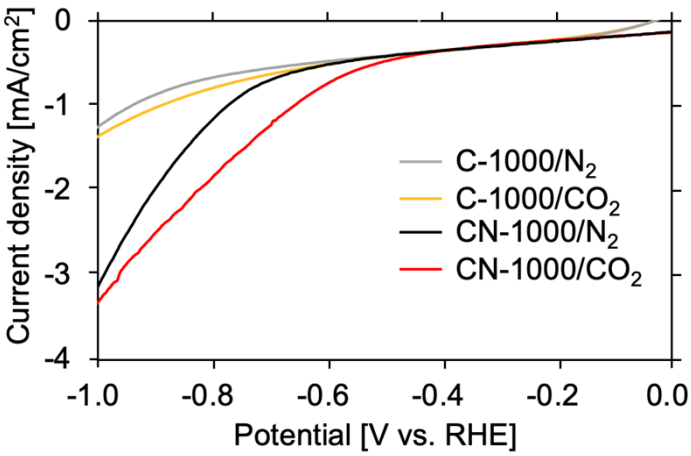

Fig. S6 LSV curves in N_2-saturated and CO_2-saturated 0.1 M $KHCO_3$ solution using C-1000 and CN-1000.

Table S2 Comparison of potential, FE_{CO}, and j_{CO} for reported metal-free carbon-based materials measured in 0.1 M $KHCO_3$ aqueous solution using an H-type cell.

Catalyst	Synthesis Procedure	Potential (V vs. RHE)	FE_{CO} (%)	j_{CO} (mA cm^{-2})	Ref.
CN-1000	Direct one-step pyrolysis of acetone-NaOH-derived precursor at 1000 °C	**-0.60**	**87.9**	**0.25**	**This Work**
DNC-1200-L	Pyrolysis of ZIF-8 followed by high-temp treatment at 1200 °C to evaporate Zn	-0.70	93.0	0.7-0.8	[5]
BNMC	Silica-templated pyrolysis of glucose, urea, dicyandiamide, and boric acid at 1000 °C	0.55	95	2.7	[6]
SeBN-C-1100	Ternary doping pyrolysis of precursors with Se, B, and N sources at 1100 °C	-0.60	95.2	0.75	[7]
NS-C-900	Two-step pyrolysis of N and S sources at 900 °C	-0.60	92.0	2.63	[8]
CB-NGC-2	Direct one-step pyrolysis of Chitin biomass, melamine and $FeCl_3$ at 900 °C	-0.56	91.0	3.7	[9]
NSHPC	Pyrolysis of glucosamine and thiocyanuric acid with SiO_2 hard templates	-0.60	87.8	~3	[10]
NF-C-950	Two-step pyrolysis of vacuum-dried N and F precursors at 950 °C	-0.60	90.0	1.90	[11]

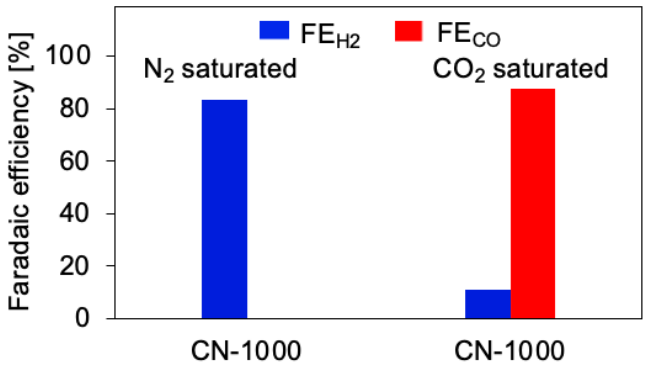

Fig. S7 Faradaic efficiency using CN-1000 (CN-1) at -0.6 V vs. RHE in N_2- or CO_2-saturated 0.1 M $KHCO_3$ solution.

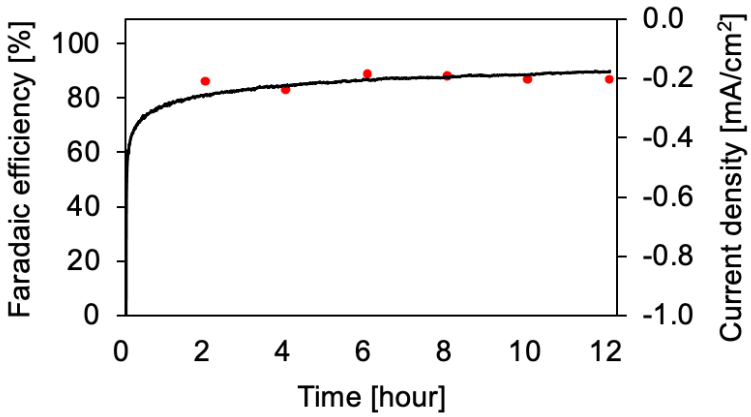

Fig. S8 Faradaic efficiencies of CO and current density using CN-1000 (CN-1) for 12 hours with the potential window at -0.6 V vs. RHE in CO_2-saturated 0.1 M $KHCO_3$ solution.

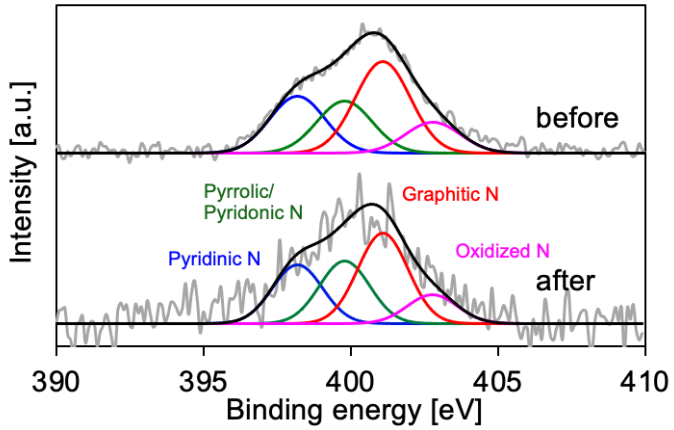

Fig. S9 XPS spectra of CN-1000 after 12h test.

Table S3 CHN analysis of CN-*T*.

Sample	C [wt%]	H [wt%]	N [wt%]
CN-1000	83.49	1.11	1.76
CN-1100	91.45	0.42	1.49
CN-1200	89.80	0.24	1.11

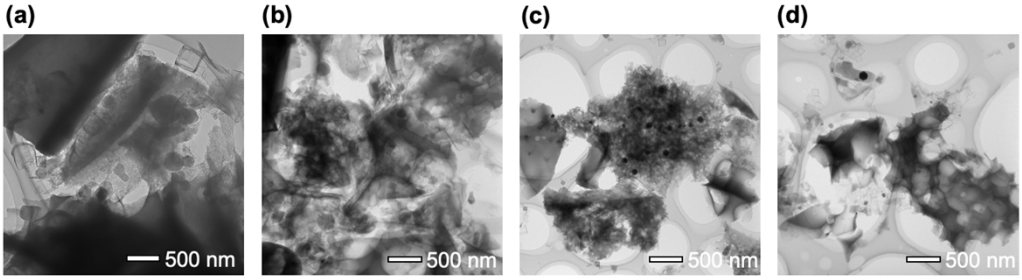

Fig. S10 TEM image of (a) CN-0.5, (b) CN-1, (c) CN-2 and (d) CN-3.

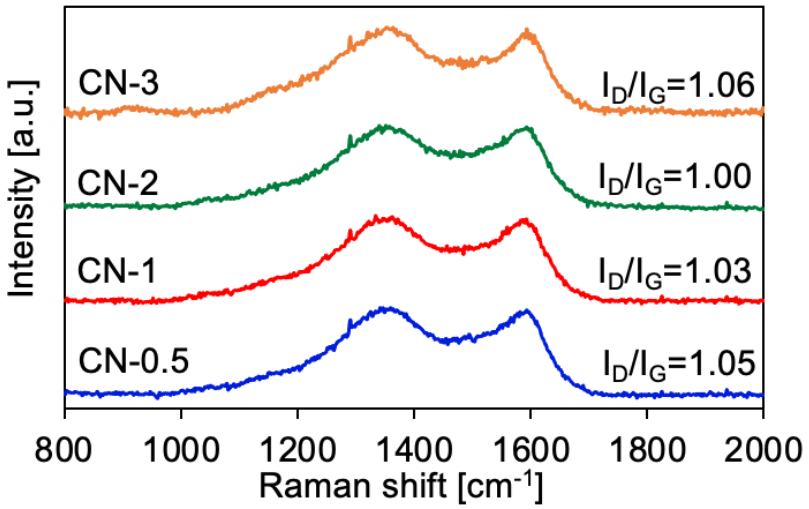

Fig. S11 Raman spectroscopy analysis of CN-*x*.

Table S4 CHN analysis of CN-*x*.

Sample	C [wt%]	H [wt%]	N [wt%]
CN-0.5	83.11	0.83	1.88
CN-1	83.49	1.11	1.76
CN-2	78.29	1.40	1.24
CN-3	80.28	1.21	1.63

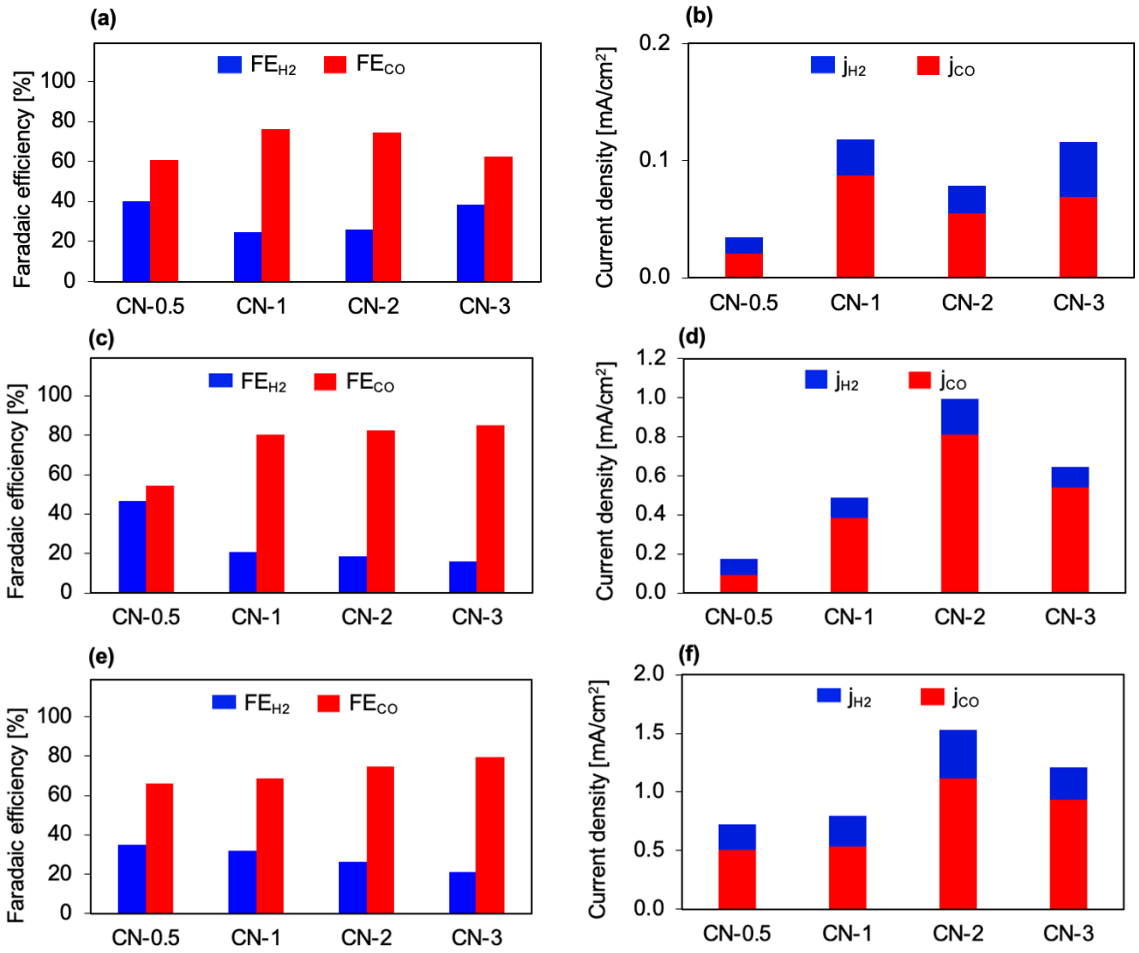

Fig. S12 (a) FE_{CO} and FE_{H2} using CN-*x* with the potential window at -0.5 V vs. RHE in CO_2-saturated 0.1 M $KHCO_3$ solution, (b) j_{CO} and j_{H2} using CN-*x* at -0.5 V vs. RHE, (c) FE_{CO} and FE_{H2} using CN-*x* with the potential window at -0.7 V vs. RHE in CO_2-saturated 0.1 M $KHCO_3$ solution, (d) j_{CO} and j_{H2} using CN-*x* at -0.7 V vs. RHE, (e) FE_{CO} and FE_{H2} using CN-*x* with the potential window at -0.8 V vs. RHE in CO_2-saturated 0.1 M $KHCO_3$ solution and (f) j_{CO} and j_{H2} using CN-*x* at -0.8 V vs. RHE.

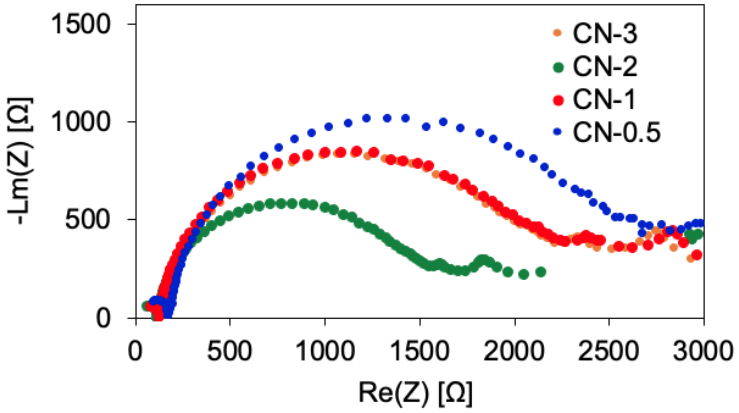

Fig. S13 Nyquist plots of CN-*x*.

Reference:

1 R. V. Siriwardane, J. A. Poston, C. Robinson and T. Simonyi, *Energy Fuels*, 2011, **25**, 1284–1293.

2 S. Kang, J. B. Park, T.-J. Lee, S. Ryu, S. H. Bhang, W.-G. La, M.-K. Noh, B. H. Hong and B.-S. Kim, *Carbon*, 2015, **83**, 162–172.

3 X. Deng, A. Verdaguer, T. Herranz, C. Weis, H. Bluhm and M. Salmeron, *Langmuir*, 2008, **24**, 9474–9478.

4 M. Gabrijelčič, B. Tratnik, G. Kapun, E. Tchernychova, N. Z. Logar, A. Krajnc, R. Dominko and A. Vizintin, *J. Mater. Chem. A*, 2025, **13**, 1042–1056.

5 R. Takada, K. Narimatsu, K. Miyake, Y. Uchida and N. Nishiyama, *ACS Appl. Energy Mater.*, 2025, **8**, 13231–13238.

6 X. Ma, J. Du, H. Sun, F. Ye, X. Wang, P. Xu, C. Hu, L. Zhang and D. Liu, *Appl. Catal. B Environ.*, 2021, **298**, 120543.

7 W. Wang, J. Han, Y. Sun, M. Zhang, S. Zhou, K. Zhao and J. Yuan, *ACS Appl. Energy Mater.*, 2022, **5**, 10518–10525.

8 F. Pan, B. Li, W. Deng, Z. Du, Y. Gang, G. Wang and Y. Li, *Appl. Catal. B Environ.*, 2019, **252**, 240–249.

9 X. Hao, X. An, A. M. Patil, P. Wang, X. Ma, X. Du, X. Hao, A. Abudula and G. Guan, *ACS Appl. Mater. Interfaces*, 2021, **13**, 3738–3747.

10 R. Li, F. Liu, Y. Zhang, M. Guo and D. Liu, *ACS Appl. Mater. Interfaces*, 2020, **12**, 44578–44587.

11 F. Pan, B. Li, X. Xiang, G. Wang and Y. Li, *ACS Catal.*, 2019, **9**, 2124–2133.